Traveltime-based true-amplitude migration

C. Vanelle, M. Spinner, T. Hertweck, C. Jäger, and D. Gajewski

email: *vanelle@dkrz.de*

keywords: *Kirchhoff Migration, True Amplitudes, Traveltimes*

ABSTRACT

True-amplitude Kirchhoff migration is a task of high computational effort. A substantial part of this effort is spent on the calculation of Greens functions, i.e. traveltime tables and amplitude-preserving weight functions. Storing the Greens functions leads to large demands in computer storage in addition to the high requirements in CPU time. In this paper we propose a strategy to compute the weight functions directly from coarsely-gridded traveltimes. Together with a fast and accurate method for the interpolation of the traveltimes onto the required fine migration grid, this leads to considerable savings in CPU time as well as storage. Application to a complex synthetic model and real data demonstrates that the image quality and accuracy of the reconstructed amplitudes is equivalent to that obtained by conventional true-amplitude Kirchhoff migration, whereas the computational efficiency is significantly enhanced.

INTRODUCTION

True-amplitude Kirchhoff migration is a powerful tool for the processing of seismic reflection data. In addition to a structural image, amplitude maps of the subsurface are obtained. These can be input for amplitude versus offset (AVO) studies, a key technique for seismic reservoir characterization. The result of a Kirchhoff migration is an image in the time or in the depth domain. In this work, we will focus on depth imaging, although the method suggested here can also be applied to obtain a time migrated section. In Kirchhoff depth migration, the subsurface is represented by a reasonably discretised grid, where every grid point is considered a point scatterer. The migration for a depth point M is carried out by stacking the seismograms along the diffraction traveltime surface associated with M and placing the result into M. If specific true-amplitude weight functions are applied during the stacking process, the effect of geometrical spreading can be removed and the migration output becomes a measure of the angle-dependent reflectivity. In most cases, the resulting amplitudes are still influenced by other effects, like transmission losses, but these are usually assumed to be of second order. During the last decades, several approaches have led to different formulations for the true-amplitude weight functions (e.g., Bleistein 1987; Schleicher et al. 1993), that can, however, be shown to be equivalent (Hanitzsch, 1997).

Despite its benefits, true-amplitude migration is not routinely applied, as it is a task of high computational effort, especially when 3D data are considered. In order to obtain a highly-resolved image, the subsurface must be finely discretised. A sampling of down to 5 m is desired, but not feasible due to the sheer amount of auxiliary data required for the migration step, namely, the traveltime surfaces and weight functions. For each point where a source or receiver is located in the registration surface a table must be generated with the traveltime to each subsurface point on the grid. For the 3D weight function, additional quantities have to be computed and stored from each source/geophone to each subsurface point. Whereas fast implementations like finite difference eikonal solvers (FDES, e.g., Vidale 1990) can be applied for the traveltimes, the computation of the weights requires more effort: since the purpose of the weight functions is the removal of the geometrical spreading determined by the curvature of the wavefront, the standard way to compute the weights is the application of dynamic ray tracing (Červený and deCastro, 1993; Hanitzsch

et al., 1994), which is more time-consuming than FDES. Finally, another part of the computational time is spent during the stacking itself, which has to be carried out over the aperture of the experiment. Since in practice only a minor part of the traces effectively contributes to the stack, the aperture is usually limited to a predefined size (see, e.g.,Hertweck et al. 2003). For these reasons, true-amplitude migration has not yet become a standard tool.

The aim of this paper is the introduction of a traveltime-based algorithm for true-amplitude migration. In this method, all quantities required for the migration weights, as well as for the stacking surface, are obtained from coarsely-gridded traveltime tables. This leads to a considerable reduction in computer storage and computation time, while maintaining the quality of the migrated image and recovered amplitudes, compared to standard true-amplitude migration using dynamic ray tracing. Although a traveltime-based strategy was already suggested by Vanelle (2002), Vanelle and Gajewski (2002b), and Gajewski et al. (2002), application of that technique still required a priori knowledge on the positions and inclinations of reflectors in the subsurface. This work does no longer suffer from that restriction.

Following a short introduction to the theory of true-amplitude migration, we will describe the traveltime-based approach. The major part of this paper is then dedicated to the application of the method to a highly-complex synthetic model and a real data set. Finally we conclude the paper with a short summary and an outlook.

METHOD

Note: Capital indices like I take the values 1 and 2, whereas small indices i take values 1, 2, and 3.

True-amplitude migration in three dimensions

Schleicher et al. (1993) have shown, that the true-amplitude migrated output $\Omega(M)$ at the subsurface point M can be obtained from a diffraction stack of the form

$$\Omega(M) = -\frac{1}{2\,\pi} \iint\limits_A \mathrm{d}\boldsymbol{\xi}\, W_{3D}(\boldsymbol{\xi}, M)\ \left.\frac{\partial U(\boldsymbol{\xi}, t)}{\partial t}\right|_{\tau_D(\boldsymbol{\xi}, M)} \quad , \tag{1}$$

if proper weight functions $W_{3D}(\boldsymbol{\xi}, M)$ are applied. The integration in (1) is carried out over the aperture A, that contains the considered traces at the positions $\boldsymbol{\xi} = (\xi_x, \xi_y)$ (see e.g. Schleicher et al. 1993). The stacking surface is the diffraction traveltime surface $t = \tau_D(\boldsymbol{\xi}, M)$ for the depth point M, calculated in a previously determined macro-velocity model. If the seismic data $U(\boldsymbol{\xi}, t)$ are expressed by (Červený, 2001)

$$U(\boldsymbol{\xi}, t) = \sqrt{\frac{\rho_s\, V_s}{\rho_g\, V_g}}\, \mathcal{R}\, \mathcal{G}_s\, \frac{\mathrm{e}^{i\frac{\pi}{2}\kappa}}{\mathcal{L}}\, F(t - \tau_R) \quad , \tag{2}$$

Schleicher et al. (1993) and Vanelle and Gajewski (2002b) have shown, that application of the weight function

$$W_{3D}(\boldsymbol{\xi}, M) = \sqrt{\frac{\rho_g\, V_g}{\rho_s\, V_s}}\, \frac{\sqrt{\cos\theta_S \cos\theta_G}}{\mathcal{G}_s}\, \frac{\left|\mathbf{N}_1^{r\top}\boldsymbol{\Sigma} + \mathbf{N}_2^{r\top}\boldsymbol{\Gamma}\right|}{|\mathbf{N}_1^r\, \mathbf{N}_2^r|}\, \mathrm{e}^{i\frac{\pi}{2}(\kappa_1+\kappa_2)} \tag{3}$$

allows to reconstruct the reflection coefficient, $\mathcal{R}$, i.e. $\Omega(M)$ yields a reflectivity map of the subsurface. In (2) and (3), ρ_s and V_s are the density and velocity at the source. Correspondigly, ρ_g and V_g are the density and velocity at the geophone. The radiation function of the source is denoted by $\mathcal{G}_s$, e.g., for P-waves an explosion source has $\mathcal{G}_s = 1/4\pi\rho_s V_s^2$, and $F(t)$ is the time signature of the analytic source pulse. The geometrical spreading is denoted by $\mathcal{L}$, the reflection traveltime by τ_R, and the angles θ_S and θ_G are the emergence angle at the source and the incidence angle at the receiver, respectively. The KMAH indices κ_1, κ_2, and κ correspond to the ray branches from the source S to M (index 1), the geophone G to M (index 2), and the reflected ray. The configuration matrices $\boldsymbol{\Sigma}$ and $\boldsymbol{\Gamma}$ describe the relations between the parameter $\boldsymbol{\xi}$ and the source $\mathbf{s}$ and geophone position $\mathbf{g}$ (Schleicher et al., 1993). Finally, the 2×2 matrices $\mathbf{N}_I^r$ are second-order derivative matrices of the traveltime,

$$N^r_{1_{IJ}} = -\frac{\partial^2 T(S, M)}{\partial s_I \partial r_J} \quad , \quad \text{and} \quad N^r_{2_{IJ}} = -\frac{\partial^2 T(G, M)}{\partial g_I \partial r_J} \quad . \tag{4}$$

The coordinates of the source and geophone are given in a global Cartesian coordinate system, e.g., chosen to coincide with the acquisition scheme, whereas the coordinates r_1 and r_2 lie in the reflector tangent plane (see Appendix A). Transmission losses are not considered in this study.

True-amplitude migration in 2.5 dimensions

In the special case where the data were aquired along a single line and the medium does not vary in the cross-line direction, the true-amplitude migration algorithm (1) can be modified and restricted to an integration over the in-line direction. The stack corresponding to (1) for this so-called 2.5D situation looks as follows, where ξ=ξ_x:

$$\Omega(M) = \frac{1}{\sqrt{2\,\pi}} \int\limits_A \mathrm{d}\xi\, W_{2.5D}(\xi, M)\ \partial_t^{-1/2} U(\xi, t)\Big|_{\tau_D(\xi,M)} \quad . \tag{5}$$

Here, the operator $\partial_t^{-1/2}$ denotes the Hilbert transform of the anti-causal temporal half-derivative of the seismic data, corresponding to the application of a $\sqrt{-i\omega}$ filter in the frequency domain. The modified weight function reads (Martins et al., 1997; Vanelle and Gajewski, 2002b)

$$W_{2.5D}(\xi, M) = \sqrt{\frac{\rho_g\, V_g}{\rho_s\, V_s}}\, \frac{\sqrt{\cos\theta_S \cos\theta_G}}{\mathcal{G}_s}\, \frac{|N_1^r \Sigma + N_2^r \Gamma|}{|N_1^r\, N_2^r|}\, \sqrt{\sigma_1 + \sigma_2}\ \mathrm{e}^{i\frac{\pi}{2}(\kappa_1+\kappa_2)} \quad , \tag{6}$$

where Σ, Γ, and N_I are the xx-components of the matrices $\mathbf{\Sigma}$, $\mathbf{\Gamma}$, and $\mathbf{N}_I$, respectively. The term $\sqrt{\sigma_1 + \sigma_2}$ is the out-of-plane geometrical spreading, where the components σ_I are given by

$$\sigma_I = \left(\frac{\partial^2 T}{\partial y_I^2}\right)^{-1} = \frac{1}{N_{I_{yy}}} \quad . \tag{7}$$

The weight functions (3) and (6) are written in terms of traveltime derivatives as these directly relate to the traveltime-based implementation suggested in this work. For other implementations the equivalent weights can be expressed by quantities available from dynamic ray tracing (for an overview, see, e.g. Hanitzsch 1997). Although the classic true-amplitude migration employs weights from dynamic ray tracing (DRT), it has not become a standard tool due to the strong requirements in computer demands (CPU time and storage) as well as on the model (continuity of second-order spatial velocity derivatives is required for DRT). As we will show in the following, the traveltime-based implementation underlies weaker restrictions.

The traveltime-based strategy

To carry out the migration using either (1) or (5) we need the weight functions (3) or (6) and the diffraction traveltime surface or curve, $\tau_D(\boldsymbol{\xi}, M)$. The diffraction traveltimes are needed anyway, even for a purely kinematic migration. If first-arrival traveltimes are considered only, these can be obtained from fast traveltime generation methods like finite difference eikonal solvers (for an overview of traveltime schemes, see Leidenfrost et al. 1999). Later-arrival traveltimes can be computed with kinematic ray tracing. For the computation of the weight functions, however, dynamic ray tracing has to be carried out even for the first arrivals.

In this section we will describe how the true-amplitude weights can be obtained from coarsely-gridded traveltime tables without further need for dynamic ray tracing. The traveltime coefficients that determine the weights are also applied for an efficient and accurate interpolation of the traveltimes onto the fine migration grid. By doing so, we can considerably reduce the computational demands and yet maintain the high quality of the migrated image.

In the following we will assume that diffraction traveltime tables sampled on a coarse subsurface grid are available. The subsurface sampling should accord with the prevailing wavelength in the data, and the model. In this case, the hyperbolic traveltime expression of Vanelle and Gajewski (2002a), obtained from a Taylor expansion of the squared traveltime,

$$T^2(\mathbf{s}, \mathbf{g}) = \left(T_0 + \mathbf{q}\cdot\mathbf{\Delta g} - \mathbf{p}\cdot\mathbf{\Delta s}\right)^2 + T_0\left(\mathbf{\Delta g}\cdot\mathbf{G}\mathbf{\Delta g} - \mathbf{\Delta s}\cdot\mathbf{S}\mathbf{\Delta s} - 2\,\mathbf{\Delta s}\cdot\mathbf{N}\mathbf{\Delta g}\right) \quad , \tag{8}$$

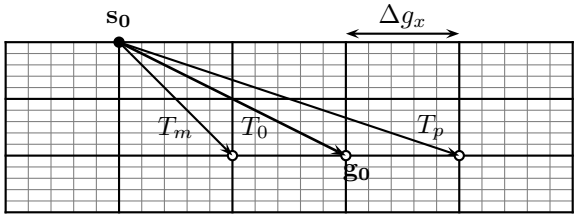

Figure 1: Determination of the coefficients from Equation (8): the traveltimes T_0, T_m, T_p on the coarse grid with the spacing Δg_x.

can be applied to describe the reflection traveltime between a source at $\mathbf{s}$ and a geophone at $\mathbf{g}$ in the vicinity of the expansion point at $\mathbf{s_0}$ and $\mathbf{g_0}$, when the coefficients in (8) are known. These are (Vanelle and Gajewski, 2002a)

$$p_i = -\frac{\partial T}{\partial s_i} \quad \text{and} \qquad q_i = \frac{\partial T}{\partial g_i} \quad , \tag{9}$$

the slowness vectors, and the second-order derivative matrices

$$\begin{aligned} S_{ij} &= -\frac{\partial^2 T}{\partial s_i \, \partial s_j} = S_{ji} \quad , \\ G_{ij} &= \frac{\partial^2 T}{\partial g_i \, \partial g_j} = G_{ji} \quad , \\ N_{ij} &= -\frac{\partial^2 T}{\partial s_i \, \partial g_j} \neq N_{ji} \quad . \end{aligned} \tag{10}$$

All derivatives are taken at the expansion point. Furthermore, T_0 is the traveltime from $\mathbf{s_0}$ to $\mathbf{g_0}$, and $\mathbf{\Delta s}$ and $\mathbf{\Delta g}$ are the distances in source and receiver position to the expansion point. The expansion points coincide with the coarse grid nodes of the traveltime tables (see Figure 1).

Vanelle and Gajewski (2002a) describe how the coefficients in the traveltime expression (8) can be obtained from coarsely-gridded traveltime tables. We give an example for the determination of the coefficients q_x and G_{xx}. Figure 1 shows a grid on which the traveltimes T_0, $T_m = T(\mathbf{s_0}, \mathbf{g_0} - \Delta g_x)$, and $T_p = T(\mathbf{s_0}, \mathbf{g_0} + \Delta g_x)$ are given. The traveltimes T_1 and T_2 are substituted into the hyperbolic expression (8):

$$\begin{aligned} T_m^2 &= (T_0 - q_x \, \Delta g_x)^2 + T_0 \, G_{xx} \, \Delta g_x^2 \\ T_p^2 &= (T_0 + q_x \, \Delta g_x)^2 + T_0 \, G_{xx} \, \Delta g_x^2 \quad . \end{aligned}$$

This resulting system of equations is solved for the two unknowns q_x and G_{xx}, leading to

$$q_x = \frac{T_p^2 - T_m^2}{4 \, T_0 \, \Delta g_x} \qquad \text{and} \qquad G_{xx} = \frac{T_p^2 + T_m^2 - 2 \, T_0^2}{2 \, T_0 \, \Delta g_x^2} - \frac{q_x^2}{T_0} \quad .$$

The coefficients q_z and G_{zz} are determined accordingly from traveltimes to $\mathbf{g_0} \pm \Delta g_z$; coefficients p_x and S_{xx} are determined using traveltimes from $\mathbf{s_0} \pm \Delta s_x$ to $\mathbf{g_0}$, and so forth. Expressions for all coefficients of (8) are given in Vanelle (2002). An investigation of the accuracy of the obtained coefficients was also carried out by Vanelle (2002).

Expression (8) is equally valid for diffraction traveltimes. The stacking surface/curve required for the summation in (1) and (5) is the sum of the traveltime from the source to the subsurface point (denoted by T_1), and, due to reciprocity, that from the geophone to the subsurface point (T_2), i.e.

$$\tau_D(\boldsymbol{\xi}, M) = T(\mathbf{s}, \mathbf{x}) + T(\mathbf{g}, \mathbf{x}) = T_1 + T_2 \quad . \tag{11}$$

The vector $\mathbf{x}$ is the position of the subsurface point M. Both T_1 and T_2 are obtained on the fine migration grid from traveltime interpolation using equation (8), as the coefficient sets for the branches 1 and 2 are determined. Note, however, that the matrices $\mathbf{N}_1$ and $\mathbf{N}_2$ are 3×3 matrices that do not coincide with the

2×2 matrices in the weight functions (3) and (6), $\mathbf{N}_1^r$ and $\mathbf{N}_2^r$: in the latter, the derivatives are taken in the reflector tangent plane, whereas $\mathbf{N}_1$ and $\mathbf{N}_2$ are defined in global Cartesian coordinates. The transformation from that system to the system defined by the reflector tangent plane is derived in Appendix A.

By applying equation (11) with hyperbolic traveltime interpolation using (8) we get the stacking surface/curve from coarsely-gridded traveltime tables. Since the position of the source can also be interpolated, we gain considerable savings in storage: if, for example, the ratio of the coarse to the fine grid spacing is ten, a factor of 10^5 can be saved in storage in 3D. Furthermore, the interpolation is very fast, and fewer traveltime tables (compared to a classic implementation) need to be computed due to the source interpolation, thus we also save in computation time. With the coefficients from equation (8) we can compute the weight functions (3) or (6); the matrices $\mathbf{N}_I^r$ are obtained from the transformation of the coefficient matrices $\mathbf{N}_I^r$ in the reflector's tangent plane (see Appendix A). Finally, the emergence angle at the source, θ_S, lies between the emerging ray and the vertical axis, and the incidence angle at the geophone, θ_G, between the incident ray and the vertical axis. They are obtained from the slowness vectors (first derivatives) by

$$\cos\theta_S = V_s\, p_{1z} \quad , \quad \text{and} \quad \cos\theta_G = V_g\, p_{2z} \quad . \tag{12}$$

As all quantities are computed *on the fly*, additional storage for the weight functions is not required. In comparison to the classic true-amplitude migration, where supplemental quantities need to be stored in addition to the traveltimes, this leads to considerable savings in storage. Furthermore, to perform dynamic ray tracing for the computation of the classic weight functions, the velocity model as well as its first- and second-order spatial derivatives must be continuous. This requirement is often not fulfilled by the output from the model building step. Here, the traveltime-based strategy has another advantage. As traveltime engines based on eikonal solvers or kinematic ray tracing only need continuity of the model up to first order, we can generate the traveltime tables with those. Although smoothing of the model may still be necessary (for a discussion on smoothing, please refer to Gajewski et al. 2002 and Gold et al. 2000), the stronger demand for continuity of second-order derivatives no longer holds.

In the following section, we will illustrate the traveltime-based algorithm with applications to a complex synthetic and a real data set. To show that the quality of the migration result is equivalent to that obtained from conventional true-amplitude migration, we compare our results to DRT-based migration.

APPLICATIONS

Synthetic data set

To investigate the performance and quality of the traveltime-based strategy to true-amplitude migration, we have chosen a complex 2.5D synthetic model, shown in Figure 2. Ray synthetic seismograms were computed using a commercial ray modelling package. Transmission losses were not modelled. A total of 56 600 traces were generated and sorted in common-offset gathers with offsets ranging from 0 to 1980 m. The resulting zero-offset section is displayed in Figure 3. Although Figure 3 reveals modelling artefacts such as missing diffractions at the pinch-outs and irregular amplitude behaviour in isolated spots, we have decided to use this highly complex model for the verification of the method, as the applicability to simple models has already been demonstrated by Vanelle and Gajewski (2002b).

Traveltime tables on coarse grids with a spacing of 100 m in each dimension were generated using ray modelling for sources distributed with a spacing of 100 m. These were the only input to the traveltime-based algorithm, together with the velocity model, that had to be slightly smoothed for the ray tracing. Only first arrivals were considered. In order to compare our method to standard weight functions, we have applied ray modelling to compute the necessary dynamic Green's functions (GFTs) on a 50 m grid with a shot spacing of also 50 m. For the 2.5D common-offset weight function (Hanitzsch, 1997) the dynamic GFT consists of the following four quantities: (1) the traveltime, (2) the emergence angle, (3) the in-plane, and (4) the out-of-plane geometrical spreading. The discretisation of the migration grid was for both methods chosen as 10 m in x- and 5 m in z-direction. This leads to savings of 95 % in memory requirements when the traveltime-based approach is applied. Note, however, that in 3D the savings can be higher. The traveltime-based migration was performed in only 13 % of the computation time required by the migration with standard weights. A purely kinematic migration (i.e. no weights were applied and traveltimes were interpolated linearly, thus needing the finer input spacing of 50 m) was about four times slower than the

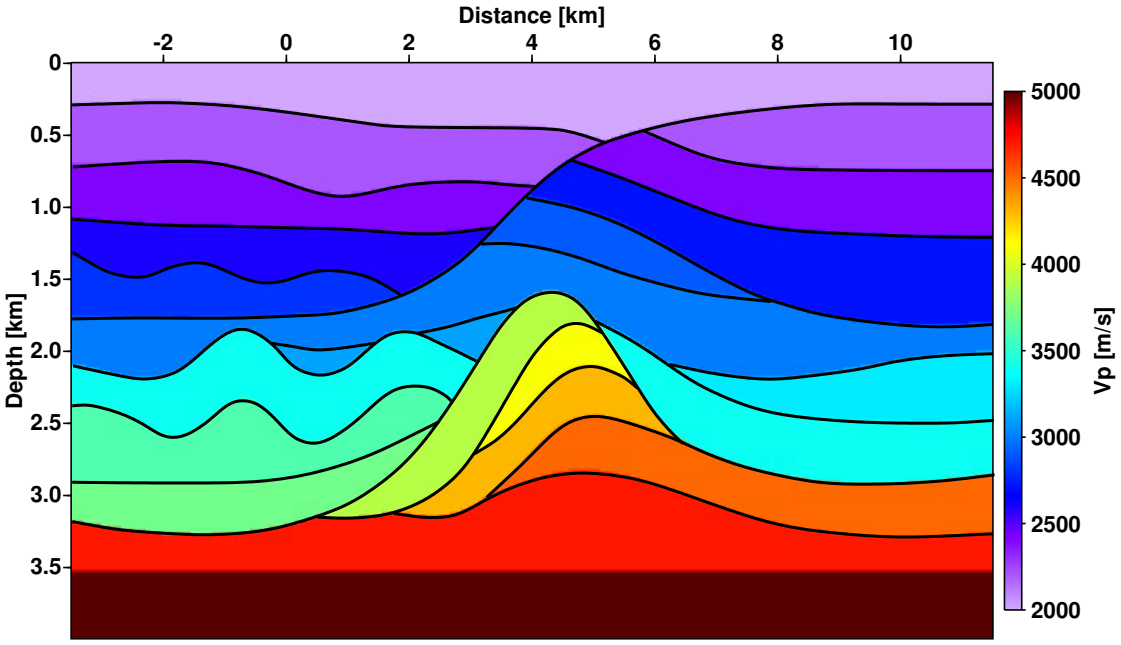

Figure 2: The velocity model for the synthetic data example. The seismograms were computed in the original blocky model shown here. For the generation of the GFTs the model was smoothed.

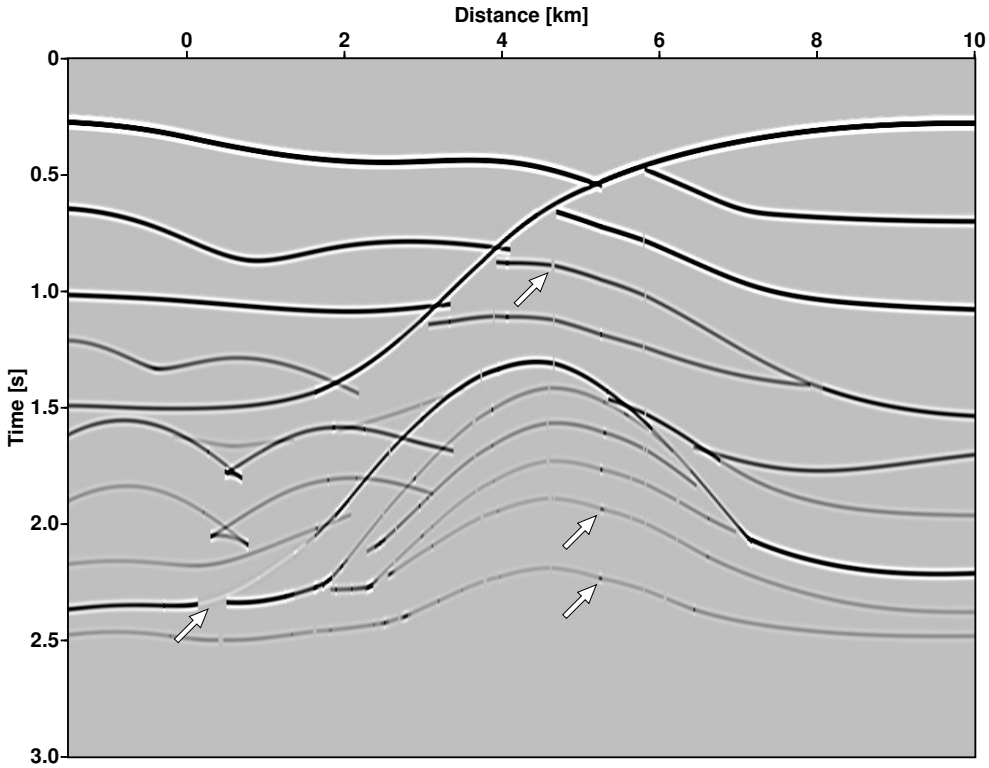

Figure 3: The (unmigrated) zero-offset section of the synthetic data set obtained by ray modelling. Note the missing diffractions at pinch-outs and changes in amplitudes along the reflectors, e.g., at the positions indicated by arrows.

traveltime-based implementation including weights. Due to the differences in the implementations, these computational times cannot be directly compared, but they indicate the efficiency of the traveltime-based method. Again, the gains will increase in 3D. In the comparison of the computational times we have not considered the fact that for the traveltime-based approach we need to generate traveltimes for less shot positions. Also, faster methods for the computation of traveltimes than dynamic ray tracing may be applied, so that the potential savings in CPU time even in 2.5D are likely to be higher than in our example.

Figure 4 shows the stacked migrated depth sections. At the shallower depths, a mute was applied to the larger offsets to avoid the distortions caused by pulse stretch. A comparison between the migration with DRT weights, Figure 4a, and traveltime-based weights, Figure 4b, reveals no obvious differences. Figure 5 displays common image gathers obtained from the migrated sections using both methods. Comparison shows no significant differences between the DRT weights (Figure 5a) and the traveltime-based weights (Figure 5b).

In addition to the structural image of the subsurface discussed in the previous paragraph, we have investigated the accuracy of the reconstructed amplitudes. Figure 6 shows a comparison of the amplitudes picked along the top (Figure 6a) and bottom (Figure 6b) reflector in the depth-migrated zero-offset section, together with the analytically computed values. For the top reflector, the recovered reflectivity from both methods coincide very well, and both agree with the analytic result. The differences between the analytic value and the migration results at the jumps in reflectivity near 5.2k m and 5.8 km can be attributed to the necessary smoothing of the velocity model and the missing diffractions (see Figure 3). For the bottom reflector, both methods still lead to coinciding results, however, they deviate from the analytic value. There are several reasons for the deviations. Although later arrivals can generally be incorporated in the traveltime-based strategy (Vanelle et al., 2003), only first arrivals are considered in the current implementation. Therefore, the energy of the later arrivals that should also contribute is missing. Also, the missing diffractions and irregular amplitude behaviour of the synthetic seismograms (see Figure 3) lead to deviations of the recovered amplitudes from the analytical values. These affect both methods in the same manner, as Figure 6 shows.

Finally, we have constructed amplitude versus offset (AVO) curves from the prestack-migrated sections for the topmost reflector at x=2.6 km. At this position, the reflector is plane and horizontal, thus we could compute the corresponding analytical reflectivity. The results are shown in Figure 7. Again, we can see that the reflectivity obtained from both migration methods coincide, and both match the analytical values very well.

Real data set

The seismic data used for the following case study were acquired by an energy resource company. They intend to carry out a project where a detailed knowledge of the subsurface structures is essential.

After standard preprocessing of the field data, an imaging workflow based on the Common-Reflection-Surface stack (CRS) (Hertweck, 2004; Mann et al., 2003) was carried out. The velocity model shown in Figure 8 was obtained from a tomographic inversion of the CRS attributes (Duveneck, 2004). This model was used to generate the input GFTs by ray modelling. For the traveltime-based migration, the ratio of the spacings between coarse input grid and migration grid was 10 in x-, and 20 in z direction. The tables were computed for every fifth source position. For the dynamic GFTs the ratio of the spacings between coarse input grid and migration grid was 4 in x- and 8 in z-direction. The GFTs were computed for every second source position.

The computational time required for the traveltime-based migration was 20 % of that using dynamic GFTs. Concerning computer storage, the traveltime-based implementation lead to savings of 96 %. Again, we expect the savings to be higher in 3D. Also, the CPU time savings do not include the savings achieved from the fact that traveltimes need to be generated for fewer shots and with a possibly faster method than dynamic ray tracing.

Figures 9 and 10 show the stacked sections and the common-image gathers obtained from the migration using both implementations. We have not investigated the amplitude behaviour further as some steps in the preprocessing applied to the field data were not preserving the amplitudes. However, as in the previous synthetic examples, the results from both methods appear virtually identical.

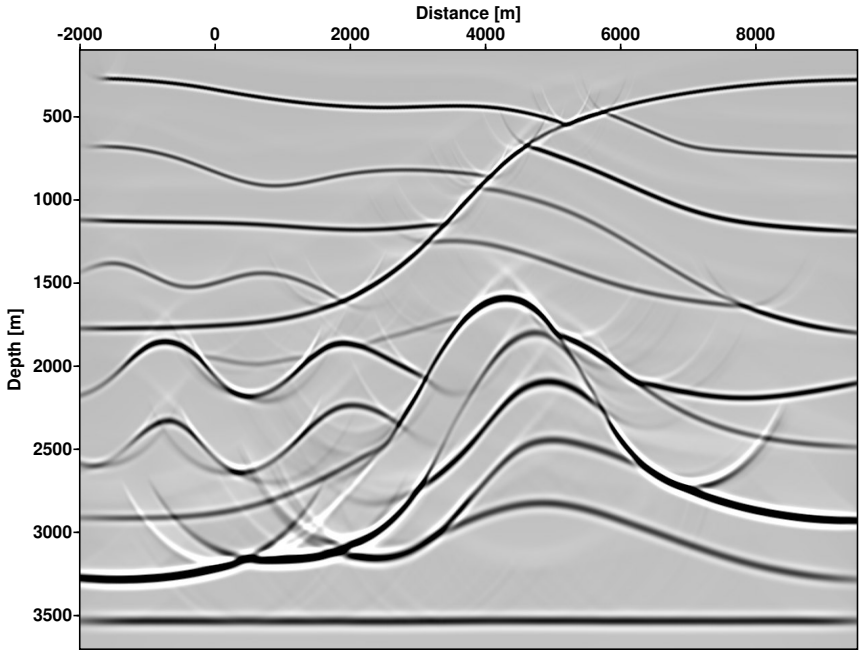

(a)

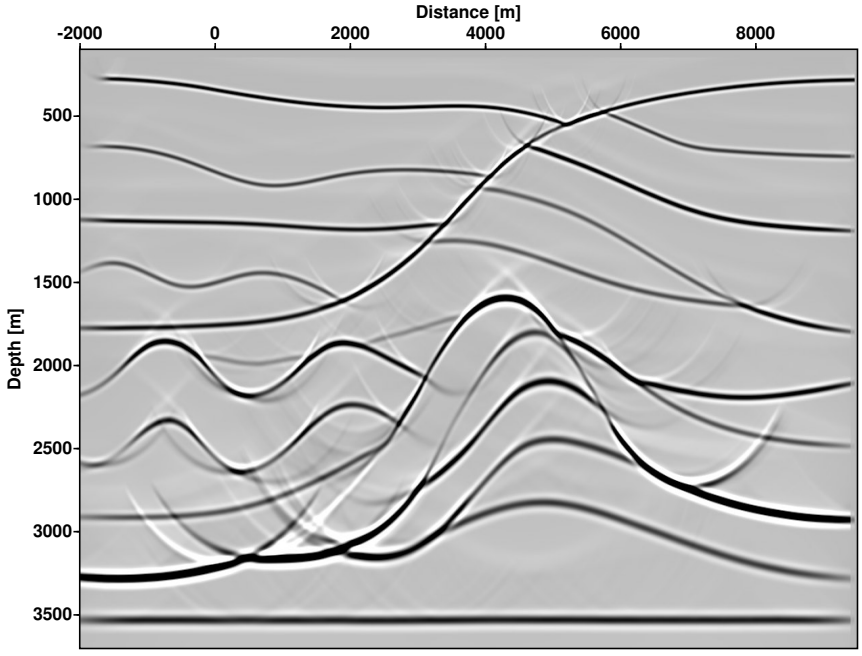

(b)

Figure 4: The true-amplitude prestack-migrated and stacked sections for the synthetic data set: (a) with weights from dynamic ray tracing, (b) from the traveltime-based approach with ray traveltimes. The diffractions at pinch-outs are artefacts due to gaps and amplitude discontinuities in the input seismograms, see Figure 3. There is no visible difference between (a) and (b).

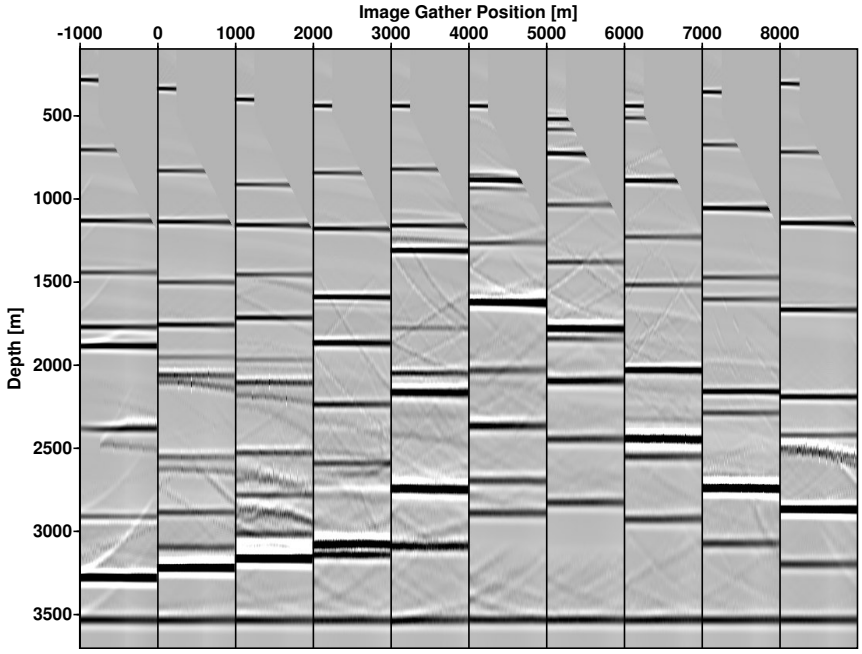

(a)

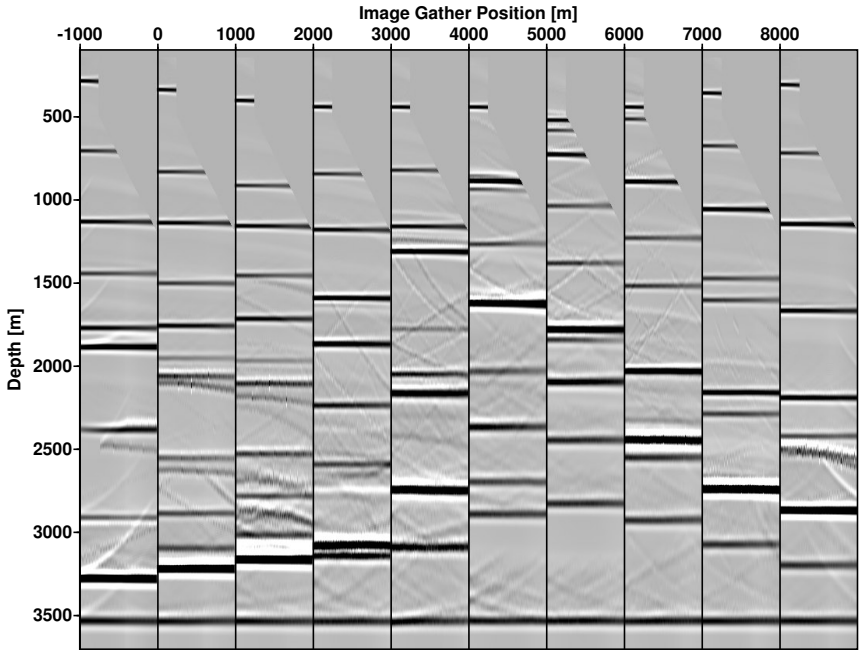

(b)

Figure 5: Common image gathers resulting from migration of the synthetic data with DRT weights (a) and traveltime-based weights (b). No apparent difference is visible.

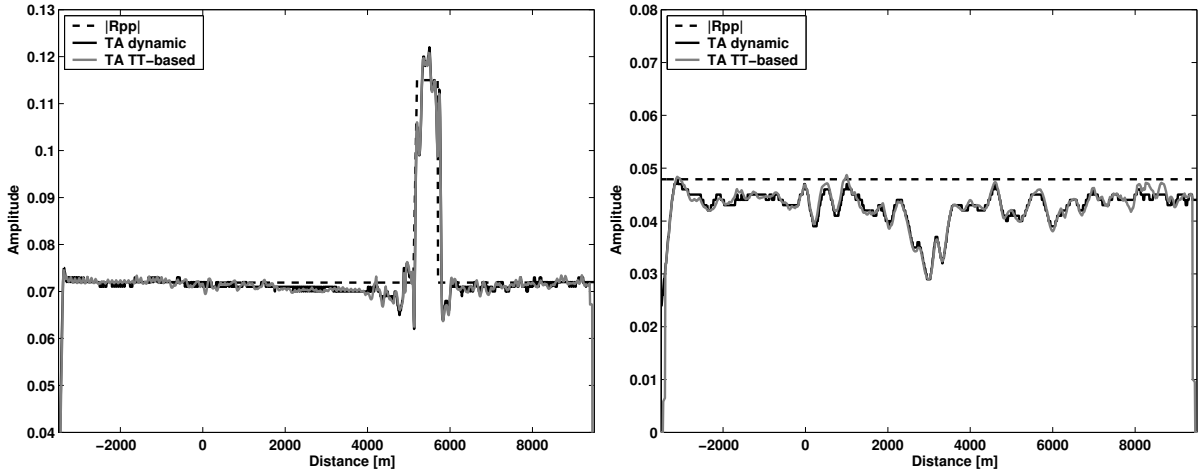

Figure 6: Amplitudes of the top (a) and bottom (b) reflector in the synthetic model picked from the migrated depth section for the zero-offset case. The results from DRT and traveltime weights coincide. The analytic reflection coefficients are also given. For the top reflector, the reflectivity could be reconstructed with higher accuracy than for the bottom reflector. The reasons are discussed in the text.

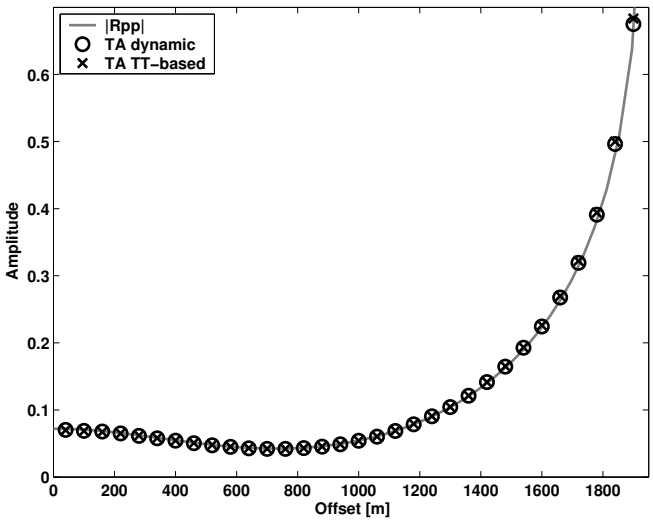

Figure 7: AVO curves for the top reflector picked from the migrated sections at x=2.6 km. At this position the reflector is horizontal, thus the incidence angle is known and a comparison to the analytic result is possible. Both migration results match the analytic values very closely.

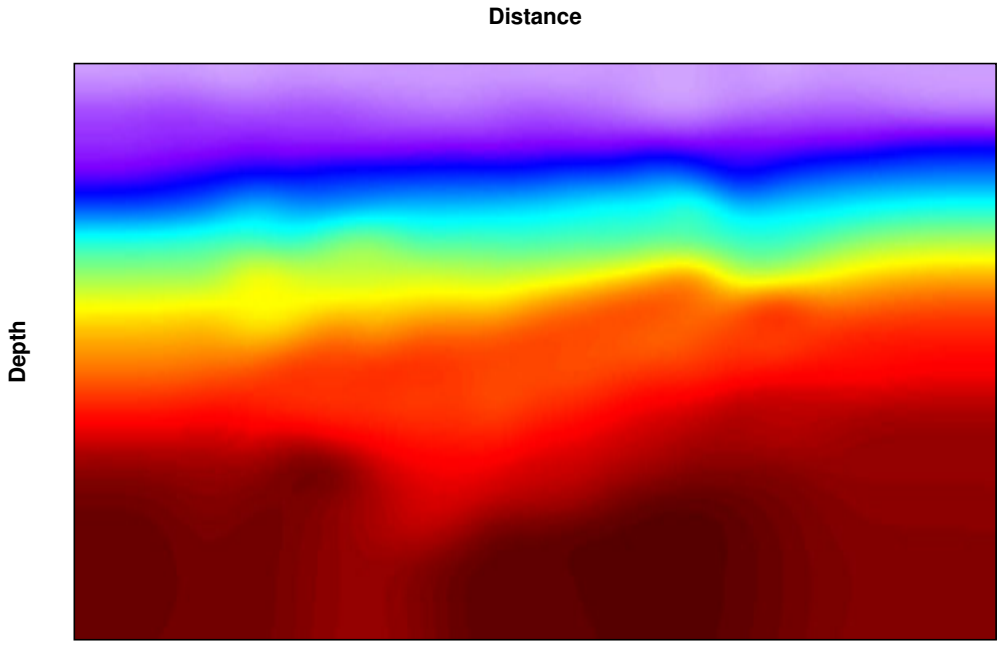

Figure 8: The velocity model for the real data set obtained from CRS tomography.

CONCLUSIONS AND OUTLOOK

We have presented a new, highly efficient traveltime-based approach to true-amplitude migration of seismic data. The method requires only traveltimes on coarse grids as opposed to the conventional true-amplitude migration, where dynamic Greens function tables must be generated on finer grids. Thus, while maintaining the quality of the resulting images and the accuracy of the recovered amplitudes, application of the traveltime-based strategy leads to considerable savings in computer storage and computational time. For the 2.5D synthetic and field data examples presented in this study, the CPU time was reduced by 80–85 %, and the required storage was reduced by about 95 % in comparison to standard true-amplitude migration, whereas no discernable differences exist between the results from both methods. We expect the savings to increase in 3D.

The new method will be even more interesting when anisotropy is considered. Whereas the requirements in computer storage do not depend on the type of medium, the computational time for the generation of the Greens function tables becomes a major issue in anisotropic media: their calculation is a magnitude slower than in isotropic media, especially when dynamic wavefield properties are concerned. Therefore, the extension of the traveltime-based strategy to account for anisotropy will lead to even higher savings than for isotropic media, as dynamic wavefield properties are no longer required. Also, traveltimes need to be calculated for fewer shots. First tests on the determination of geometrical spreading – a key quantity for the weight functions – from traveltimes in anisotropic media confirm the high potential of the technique (Vanelle and Gajewski, 2003). More details on the anisotropic extension of the traveltime-based strategy will be given in a follow-up paper.

ACKNOWLEDGEMENTS

We thank the members of the Applied Geophysics Groups in Hamburg and Karlsruhe for continuous discussions. This work was partially supported by the German Research Foundation (DFG, grants Va207-3 and Ga350-10) and the sponsors of the Wave Inversion Technology (WIT) Consortium. We are grateful to the energy resource company for providing the real data set.

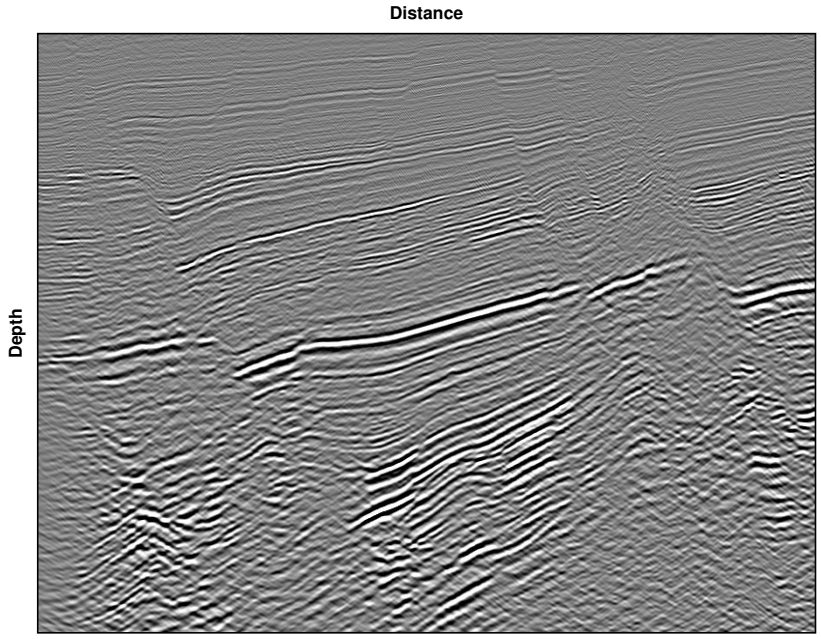

(a)

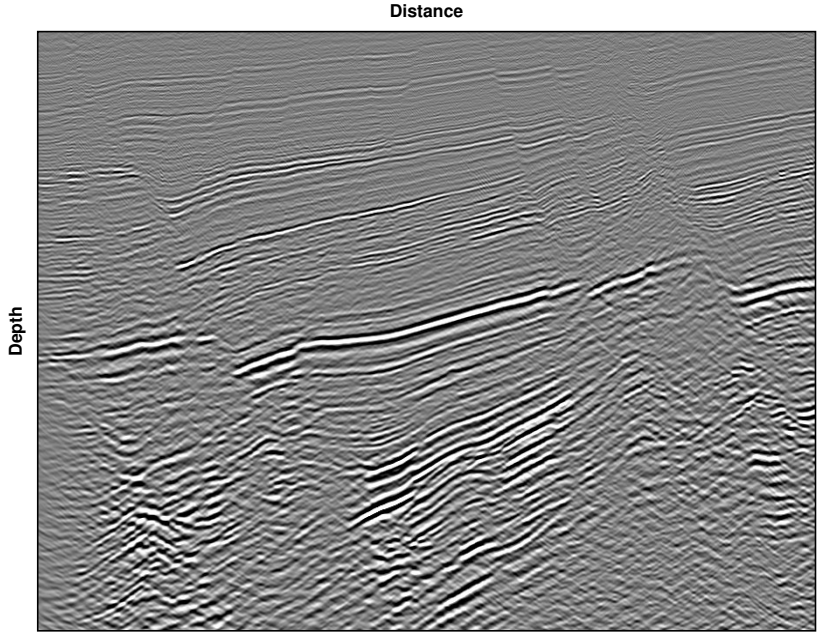

(b)

Figure 9: The true-amplitude migrated and stacked sections of the real data set: (a) with weights from dynamic ray tracing, (b) from the traveltime-based approach with ray traveltimes for the real data model. There is no visible difference between (a) and (b).

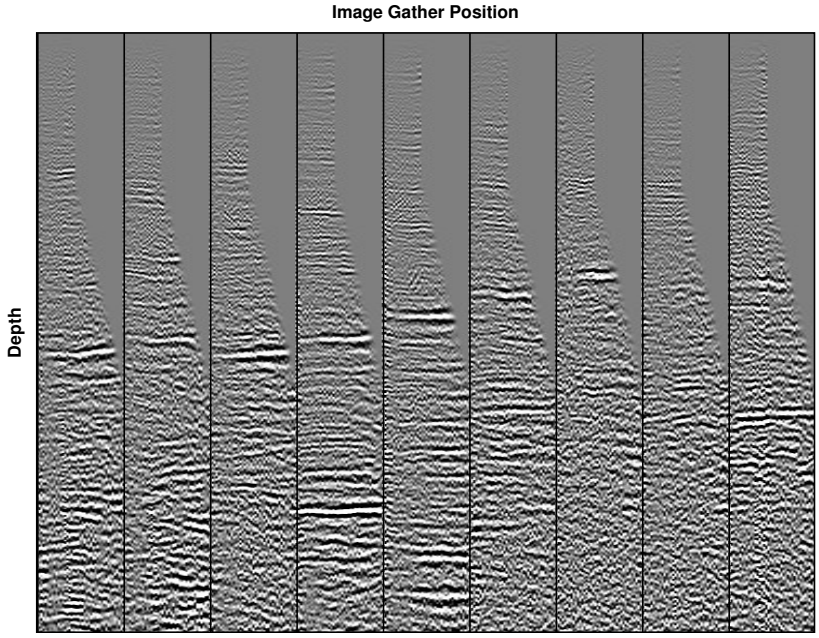

(a)

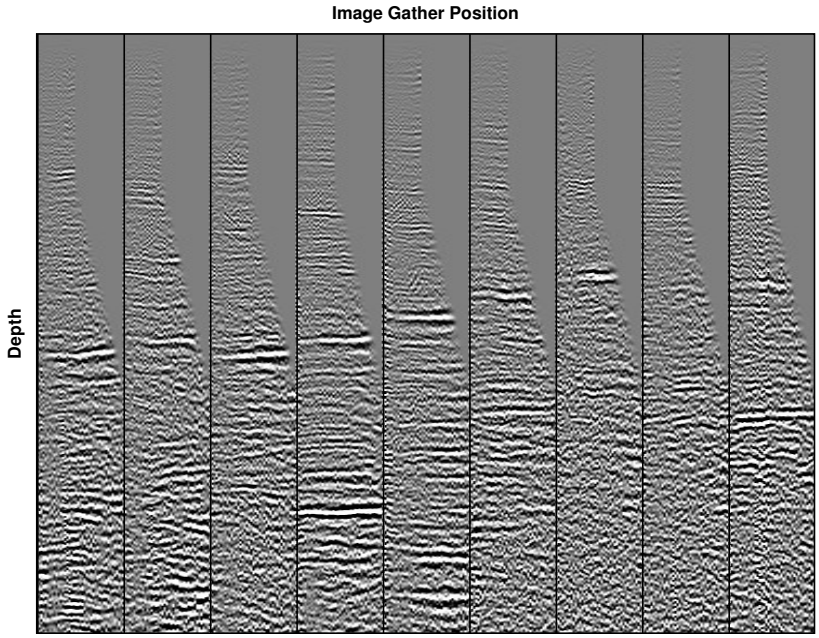

(b)

Figure 10: Common image gathers resulting from migration of the real data with DRT weights (a) and traveltime-based weights (b) for the real data model. No apparent difference is visible.

REFERENCES

Bleistein, N. (1987). On the imaging of reflectors in the earth. *Geophysics*, 52:931–942.

Červený, V. (2001). *Seismic Ray Theory*. Cambridge University Press.

Červený, V. and deCastro, M. A. (1993). Application of dynamic ray tracing in the 3-D inversion of seismic reflection data. *Geophysical Journal International*, 113:776–779.

Duveneck, E. (2004). Velocity model estimation with data-derived wavefront attributes. *Geophysics*, 69:265–274.

Gajewski, D., Coman, R., and Vanelle, C. (2002). Amplitude preserving Kirchhoff migration: a traveltime based strategy. *Studia geophysica et geodaetica*, 46:193–211.

Gold, N., Shapiro, S. A., Bojinski, S., and Müller, T. M. (2000). An approach to upscaling for seismic waves in statistically isotropic heterogeneous elastic media. *Geophysics*, 65:1837–1850.

Hanitzsch, C. (1997). Comparison of weights in prestack amplitude-preserving depth migration. *Geophysics*, 62:1812–1816.

Hanitzsch, C., Schleicher, J., and Hubral, P. (1994). True-amplitude migration of 2D synthetic data. *Geophysical Prospecting*, 42:445–462.

Hertweck, T. (2004). *True-amplitude Kirchhoff migration: analytical and geometrical considerations*. PhD thesis, Logos-Verlag Berlin.

Hertweck, T., Jäger, C., Goertz, A., and Schleicher, J. (2003). Aperture effects in 2.5D Kirchhoff migration: A geometrical explanation. *Geophysics*, 68:1673–1684.

Leidenfrost, A., Ettrich, N., Gajewski, D., and Kosloff, D. (1999). Comparison of six different methods for calculating traveltimes. *Geophysical Prospecting*, 47:269–297.

Mann, J., Duveneck, E., Hertweck, T., and Jäger, C. (2003). A seismic reflection imaging workflow based on the Common Reflection Surface stack. *Journal of Seismic Exploration*, 12:283–295.

Martins, J. L., Schleicher, J., Tygel, M., and Santos, L. (1997). 2.5-D true-amplitude migration and demigration. *Journal of Seismic Exploration*, 6:159–180.

Schleicher, J., Tygel, M., and Hubral, P. (1993). 3D true-amplitude finite-offset migration. *Geophysics*, 58:1112–1126.

Vanelle, C. (2002). *Traveltime-based True-amplitude Migration*. PhD thesis, University of Hamburg.

Vanelle, C., Dettmer, J., and Gajewski, D. (2003). Detection of caustics and interpolation of later-arrival traveltimes. In *Expanded Abstracts*, pages P–048. Eur. Assn. Expl. Geophys.

Vanelle, C. and Gajewski, D. (2002a). Second-order interpolation of traveltimes. *Geophysical Prospecting*, 50:73–83.

Vanelle, C. and Gajewski, D. (2002b). True amplitude migration weights from traveltimes. *Pure and Applied Geophysics*, 159:1583–1599.

Vanelle, C. and Gajewski, D. (2003). Determination of geometrical spreading from traveltimes. *Journal of Applied Geophysics*, 54:391–400.

Vidale, J. (1990). Finite-difference calculation of traveltimes in three dimensions. *Geophysics*, 55:521–526.

APPENDIX A – TRANSFORMATION TO REFLECTOR COORDINATES

The 2×2 matrices $\mathbf{N}_1^r$ and $\mathbf{N}_2^r$ in the weight function (3) are taken in the reflector coordinate system, whereas the 3×3 matrices determined from traveltimes, $\mathbf{N}_1$ and $\mathbf{N}_2$, are given in the global Cartesian coordinate system. In this appendix we derive the transformation from global Cartesian to reflector coordinates.

We do not a priori know the orientation of the reflector element, thus this coordinate system is also unknown. In fact, we do not even know if a reflector exists at the subsurface point under consideration. However, as the migration result $\Omega(M)$ only exists if the image point M is a reflection point and the weights are taken in the stationary point, we assume that the two rays which connect S to M and G to M correspond to a specular reflection.

Let the base vectors of the global Cartesian system be denoted by $\mathbf{e}_x$, $\mathbf{e}_y$, and $\mathbf{e}_z$. We now define the base vectors of the reflector coordinate system as follows:

- Vector $\mathbf{e}_3$ is normal to the interface and given by

$$\mathbf{e}_3 = \frac{V_2\,\mathbf{q}_2 + V_1\,\mathbf{q}_1}{|V_2\,\mathbf{q}_2 + V_1\,\mathbf{q}_1|} \quad ,$$

  where V_1 and V_2 are velocities at the image point: V_1 is the velocity for the ray that connects the source and the image point, and V_2 is the velocity for the ray connecting the geophone and the image point. For pure modes it follows that $V_1 = V_2$.

- Vector $\mathbf{e}_2$ is perpendicular to the plane of incidence,

$$\mathbf{e}_2 = \frac{\mathbf{q}_2 \times \mathbf{q}_1}{|\mathbf{q}_2 \times \mathbf{q}_1|} \quad .$$

  For the zero-offset ray, where $V_1\,\mathbf{q}_1$ and $V_2\,\mathbf{q}_2$ coincide, the vector $\mathbf{e}_2$ is chosen arbitrarily in the plane perpendicular to $V_I\,\mathbf{q}_I$.

- Vector $\mathbf{e}_1$ lies along the reflector in the plane of incidence,

$$\mathbf{e}_1 = \mathbf{e}_2 \times \mathbf{e}_3 \quad .$$

The transformation from reflector coordinates, $\mathbf{r}$, to global Cartesian coordinates, $\mathbf{x}$, is then described by

$$\mathbf{r} = \mathbf{H}\mathbf{x} \quad ,$$

where the transformation matrix $\mathbf{H}$ is

$$\mathbf{H} = \begin{pmatrix} \mathbf{e}_1 \cdot \mathbf{e}_x & \mathbf{e}_1 \cdot \mathbf{e}_y & \mathbf{e}_1 \cdot \mathbf{e}_z \\ \mathbf{e}_2 \cdot \mathbf{e}_x & \mathbf{e}_2 \cdot \mathbf{e}_y & \mathbf{e}_2 \cdot \mathbf{e}_z \\ \mathbf{e}_3 \cdot \mathbf{e}_x & \mathbf{e}_3 \cdot \mathbf{e}_y & \mathbf{e}_3 \cdot \mathbf{e}_z \end{pmatrix} \quad .$$

The 2×2 matrices $\mathbf{N}_I^r$ are then obtained from

$$\mathbf{N}_I^r = \mathbf{I}_{2\times3}\mathbf{N}_I\mathbf{H}^{-1}\mathbf{I}_{3\times2} \quad ,$$

with

$$\mathbf{I}_{2\times3} = \begin{pmatrix} 1 & 0 & 0 \\ 0 & 1 & 0 \end{pmatrix} \quad \text{and} \quad \mathbf{I}_{3\times2} = \begin{pmatrix} 1 & 0 \\ 0 & 1 \\ 0 & 0 \end{pmatrix} \quad .$$